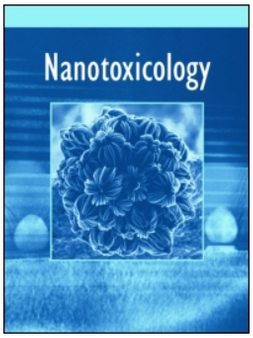

Nanotoxicology

ISSN: 1743-5390 (Print) 1743-5404 (Online) Journal homepage: http://www.tandfonline.com/loi/inan20

CARBON NANOPOWDER ACTS AS A TROJAN-HORSE FOR BENZO(α)PYRENE IN Danio rerio EMBRYOS

A. Binelli, L. Del Giacco, N. Santo, L. Bini, S. Magni, M. Parolini, L. Madaschi, A. Ghilardi, D. Maggioni, M. Ascagni, A. Armini, L. Prosperi, C. Landi, C. La Porta & C. Della Torre

To cite this article: A. Binelli, L. Del Giacco, N. Santo, L. Bini, S. Magni, M. Parolini, L. Madaschi, A. Ghilardi, D. Maggioni, M. Ascagni, A. Armini, L. Prosperi, C. Landi, C. La Porta & C. Della Torre (2017): CARBON NANOPOWDER ACTS AS A TROJAN-HORSE FOR BENZO(α)PYRENE IN Danio rerio EMBRYOS, Nanotoxicology, DOI: 10.1080/17435390.2017.1306130

To link to this article: http://dx.doi.org/10.1080/17435390.2017.1306130

Accepted author version posted online: 13 Mar 2017.

CARBON NANOPOWDER ACTS AS A TROJAN-HORSE FOR BENZO(α)PYRENE IN *Danio rerio* EMBRYOS

Binelli[1*], A., Del Giacco[1], L., Santo[1], N., Bini[2], L., Magni[1], S., Parolini[1], M., Madaschi[1], L., Ghilardi[1], A., Maggioni[3], D., Ascagni[1], M., Armini[2], A., Prosperi[1], L., Landi[2], C., La Porta[1], C., Della Torre[1**], C.

[1]Department of Biosciences, University of Milan, Via Celoria 26, 20133 Milan, Italy
[2]Department of Life Science, University of Siena, Via Aldo Moro 2, 53100 Siena, Italy
[3]Department of Chemistry, University of Milan, Via Golgi 19, 20133 Milan, Italy

Abstract

Carbon-based nanoparticles are largely distributed worldwide due to fossil fuel combustion and their presence in many consumer products. In addition to their proven toxicological effects in several biological models, attention in recent years has focused on the role played by carbon-based nanoparticles as Trojan-horse carriers for adsorbed environmental pollutants. This role has not been conclusively determined to date because carbon-based nanoparticles can decrease the bioavailability of contaminants or represent an additional source of intake. Herein, we evaluated the intake, transport and distribution of one of the carbon-based powders, the so-called carbon nanopowder, and benzo(α)pyrene, when administered alone and in co-exposure to *Danio rerio* embryos. Data obtained by means of advanced microscopic techniques illustrated that the "particle-specific" effect induced a modification in the accumulation of benzo(α)pyrene, which is forced to follow the distribution of the physical pollutant instead of its natural bioaccumulation. The combined results from functional proteomics and gene transcription analysis highlighted the different biochemical pathways involved in the action of the two different contaminants administered alone and when bound together. In particular, we observed a clear change in several proteins involved in the homeostatic response to hypoxia only after exposure to the carbon nanopowder or co-exposure to the mixture, whereas exposure to benzo(α)pyrene alone mainly modified structural proteins. The entire dataset suggested a Trojan-horse mechanism involved in the biological impacts on *Danio rerio* embryos especially due to different bioaccumulation pathways and cellular targets.

Keywords: nanoparticles, zebrafish, proteomics, microscopy, pollution

*Corresponding Author: Andrea Binelli, Department of Biosciences, University of Milan, Via Celoria 26, 20133 Milan (Italy), phone: ++39 02 50314714, e-mail: andrea.binelli@unimi.it
** Co-corresponding Author: Camilla Della Torre, Department of Biosciences, University of Milan, Via Celoria 26, 20133 Milan (Italy), phone ++39 02 50314721, e-mail: Camilla.dellatorre@unimi.it

Introduction

Carbon-based nanoparticles (CBNs) are generated and widely used in many industrial processes and products, as well as unintentionally generated as result of the incomplete combustion of fossil fuels and biomass burning. These particles are an important PM 2.5 component (Ni et al., 2014) and the second strongest global warming contributor only after CO_2 (Shrestha et al., 2010). Their presence in many consumer products and improper disposal is causing a large and increasing release to terrestrial and aquatic environments. The widespread distribution of CBNs causes harmful effects not only at the ecosystem level but also to human health, mainly depending on the intrinsic features of the particles, such as their dimension, charge, shape and aggregation behaviour (Perez, 2009). Moreover, it has been suggested that CBNs' toxicity could be increased by contaminants adsorbed to their surface (Nowack and Bucheli, 2007). Indeed, some studies highlighted that CBNs adsorb several classes of organic pollutants, such as pesticides, herbicides, benzene derivatives and pharmaceutical compounds (Cornelissen et al., 2004; Koelmans et al., 2006; Ali et al., 2015). Among these pollutants, polycyclic aromatic hydrocarbons (PAHs) are one of the major impurities adsorbed to CBNs, accounting for 39-75% of organic chemicals extractable by solvents (Watson and Valberg, 2001). Although this complication is crucial to the toxicity assessment of CBNs, to date, few studies have investigated the relationship between CBNs with organic compounds and the toxicological consequences to organisms (Canesi et al., 2015 and references therein). This combination can both amplify and decrease the toxicity of the adsorbed pollutants as a result of two possible pathways in the ternary system of CBNs-pollutant-organism. CBNs may adsorb the pollutant, reducing its free concentration in the environment, its bioavailability and consequently the toxicity. By contrast, if the CBNs with the adsorbed chemical are taken up by organisms, a toxic effect caused by the CBNs, the pollutant or the synergism of the two could result (Nowack and Bucheli, 2007). Therefore, nanoparticles (NPs) might serve as Trojan-horse-type carriers, favouring the transport of adsorbed chemicals by different routes of exposure that can change the behaviour of pollutants in organisms. The Trojan-horse mechanism was first postulated by Limbach and collaborators (2007) and then extended as possible changes in bioavailability/bioconcentration/toxicity due to NP-pollutant interactions (Baun et al., 2008). Wang and co-workers (2013) emphasised a Trojan-horse effect also on different biochemical pathways involving chemicals adsorbed on NPs and simultaneously present in cells.

In the present study, we investigated whether one of the specific carbon-based powders, the carbon nanopowder (CNPW), mediates a Trojan-horse mechanism with benzo(α)pyrene [B(α)P] using zebrafish (*Danio rerio*) embryos. We plan to employ zebrafish embryos as *in vivo* biological model since this freshwater fish has recently come to attention as a powerful vertebrate system to study several biological issues in (eco)toxicology. In fact, it represents not only an ideal biological model to evaluate the intake, accumulation and effects of some environmental pollutants, but zebrafish has recently become an ideal vertebrate animal

system also to extrapolate the toxicological results on human health (Hill et al., 2005). Moreover, the completed zebrafish sequenced genome allows the easy application of the omics techniques, such as genomics and proteomics. Finally, the zebrafish embryos are able to readily absorb contaminants, can live in 96-well plates, decreasing in this way the amount of tested substances, and all common vertebrate organs are visible after only 24 hours post fertilization (hpf; Kimmel et al., 1995). We selected the B(α)P as contaminant to add on CNPW because it is highly present in the urban areas, when it can bind to the atmospheric particulate and be subsequently introduced in organisms by respiration. Thus, B(α)P is one of the main pollutants found onto CBNs, which can represent a preferential vehicle to pass the biological barriers. Lastly, we have opted for this environmental contaminant due to its riskiness, since it is listed in the Group 1 (carcinogenic for humans) by the IARC (2010) since its metabolites are mutagenic and highly carcinogenic (Baird et al., 2005).

One of the crucial points of this study was the choice of an experimental design different from the classical plan, in which the physical and chemical compounds are supplied contemporarily but separately to the biological model. On the contrary, we created a CNPW doped with a specific quantity of B(α)P through a preliminary clean-up of the CNPW, eliminating the previously adsorbed PAHs, followed by doping of the clean CNPW with B(α)P. This foresight allowed us to assess the fate and effects of B(α)P exclusively adsorbed on the CNPW without any interference due to the hydrocarbon dissolved in water. Then, we observed by light microscopy and advanced microscopy techniques the possible capability of the CNPW, administered alone and in co-exposure with B(α)P, to enter in zebrafish embryos and eventually to translocate to other tissues. Moreover, in order to investigate the biological impact of individual contaminants and co-exposure, we carried out functional proteomics to evaluate the induced proteome changes and affected biochemical pathways and to suggest possible mechanisms of action in combination with gene expression analysis.

Materials and methods

The whole project design is shown in Figure S1, detailing every step carried out in the clean-up of the CNPW, the adsorption of B(α)P and the exposure conditions of the zebrafish embryos.

Materials

CNPW was purchased from Sigma-Aldrich (Steinheim, Germany; CAS n. 7440-44-0) with a stated particle size of <50 nm (TEM) and trace-metal purity ≥99%. All solvents used for the PAH determinations were of pesticide grade and purchased from Sigma-Aldrich (Milan, Italy). The B(α)P and PAH (PAH-Mix 14) standards were supplied by Dr. Ehrenstorfer (Augsburg, Germany).

Clean-up of CNPW

CNPW was first cleaned with 100 mL of toluene in a Soxhlet apparatus (FALC Instrument, Milan, Italy) for 92 h. Toluene aliquots (100 mL) were recovered at t=24, 48, 52 and 92 h. We added 20 mL of isooctane to each sample, which was then reduced to 1 mL and analysed on a Trace GC Ultra gas chromatograph equipped with a Polaris Q mass spectrometer (Thermo-Finnigan, Austin, Texas, USA) in SIM (selected-ion monitoring) mode. We obtained different elimination curves for every measured PAH until 92 h of clean-up.

Preparation of CNPW suspensions and B(α)P adsorption

The cleaned-up CNPW (1 g/L) was then suspended in 500 mL of MilliQ water and stirred for 48 h at 20 °C. Two different suspensions were then sonicated by a probe sonicator (Stimin s.a.s, Giussano, Italy) for 15 min at 12 kHz. The first was doped with 1 mg/L B(α)P, and the second was not contaminated. The two suspensions were stirred for 48 h at 20 °C in the dark and then centrifuged at 3,000 x g for 30 min. The supernatants were removed and stored at 4 °C, whilst the precipitated CNPW was completely dried in a muffle furnace at 40 °C for 3-4 days and stored in a desiccator.

To determine the amount of B(α)P adsorbed on CNPW, 100 mg of CNPW and CNPW+ B(α)P were extracted for 24 h in a Soxhlet apparatus. Then, each sample was processed according to the same analytical and instrumental procedures described above.

The amount of B(α)P dissolved in water was measured by liquid/liquid extraction. First, we added 100 mL of n-hexane to the supernatants. These solutions were then stirred for 90 min at 20 °C in the dark and transferred to a glass separation flask. The solvent was recovered in amber vials and then evaporated to 1 mL. The vials were maintained at -20 °C until GC-MS/MS analyses.

CNPW characterization

The primary particle diameter and shape were determined by TEM (Transmission Electron Microscope) and SEM (Scanning Electron Microscope). The morphology and purity of the bulk form were analysed using a SEM coupled with a detector for energy-dispersive X-ray (EDX) spectroscopy. The hydrodynamic diameters and surface charges (ζ potentials) of CNPW and CNPW+B(α)P were determined by DLS (dynamic light scattering). See Supplementary files for details.

Zebrafish husbandry and embryo exposure

Zebrafish of the AB strain were maintained at 28 °C on a 14-hour light/10-hour dark cycle at the Department of Biosciences of the University of Milan. Our facility strictly complies with the relevant Italian laws, rules and regulations (Legislative Decree No. 116/92), as confirmed by the authorization issued by the municipality of Milan (Art. 10 of Legislative Decree No. 116, dated 27.1.1992).

The embryos were collected by means of natural spawning and staged according to Kimmel et al. (1995). To avoid any physical interference with the uptake of the CNPW, the chorion was removed by enzymatic reaction with pronase (0.5 mg/mL) at 24 hpf prior to exposure. Dechorionated embryos were exposed in Petri dishes (4 mL) to B(α)P (20 μg/L; dissolved in dimethylsulphoxide, DMSO) and CNPW (50 mg/L) alone or in co-exposure (50 mg/L CNPW + 20 μg/L B(α)P). The chosen 50 mg/L CNPW concentration did not produce mortality or any apparent morphological or behavioural alterations. The 20 μg/L B(α)P was based on the measured effective adsorption of B(α)P on CNPW (see Results).

CNPW and B(α)P control embryos were maintained in zebrafish water (zfw) or zfw+vehicle (0.1% DMSO), respectively. The exposure continued at 28 °C until 96 hpf under semistatic conditions, replacing the solutions and contaminants every 24 h. The embryos were collected at 96 hpf and stored at -80 °C for functional proteomic and gene transcription analyses. For TEM ultrastructural analysis, control and exposed embryos were fixed in a mixture of 4% paraformaldehyde and 2% glutaraldehyde in a 0.1 M sodium cacodylate-buffered solution at pH 7.4.

For CNPW and B(α)P visualization in tissues, embryos were exposed in zfw containing 0.003% 1-phenyl 2-thiourea (PTU) to prevent pigmentation. At the end of the exposure, the embryos were fixed in 4% paraformaldehyde in a phosphate-buffered solution at pH 7.4. The experiments were performed at least 3 times for each analysis.

Histopathological and immunofluorescence analyses

Histopathological analyses were assessed by TEM in ultra-thin sections (≈70 nm) of gills, nasal fossae, digestive tract and dorsal muscle of embryos at 96 hpf (n=10 for each experimental group) for CNPW, B(α)P and CNPW+B(α)P treatments. The sections were not counterstained to avoid interference with CNPW visualization. ESI analysis was performed to confirm the nature of element signals based on the composition of the material visualized in the tissues. Immunofluorescence were conducted on cryostat sections (10 μm) of gills, yolk and digestive tract of embryos at 96 hpf (n=7 for each treatment). We used an anti-PAH primary antibody and the goat anti-mouse secondary antibody to observe the B(α)P accumulated in tissues by a confocal microscope, while CNPW was visualized in reflection mode. See Supplementary files for details.

Functional proteomics analyses

We followed the protocol reported by Riva et al. (2011), conveniently modified for zebrafish. Briefly, the zebrafish embryos (n=30 for each exposure) were homogenized in 400 μL of ice-cold buffer; 200 μg of proteins for each sample were precipitated using a chloroform/methanol/water mixture (4:1:3 v/v) and resolubilized in an adequate buffer. The first dimension (1-DE) was achieved using 18 cm of pH 3–10 non-linear gradient IPG strips (GE Healthcare, Milan, Italy) and an Ettan IPGphor II system (GE Healthcare, USA). The strips were then loaded onto a 12% acrylamide gel (24 cm length, 1 mm thickness) and run in an Ettan DALTsix electrophoresis unit (GE Healthcare). We dyed the gels with silver

stain (ProteoSilver Plus Silver Stain Kit; Sigma Aldrich). Gel images were acquired by an ImageScanner II and analysed by ImageMaster 2D Platinum software (Amersham Biosciences, USA). The spots corresponding to differentially expressed proteins were statistically evaluated in terms of the mean relative volume using Student's t-test for unpaired samples after testing for normality (Shapiro–Wilk W-test) and homogeneity of variance (Levene's test) by using STATISTICA 7.0 software package. The significance level was defined as $p<0.05$. To avoid obtaining false significance, a minimum 2-fold change cut-off relative to the controls was employed as a further criterion for differential expression.

The proteins were identified by MALDI-TOF/TOF (matrix-assisted laser desorption/ionization-time of flight/time of flight) mass spectrometry. Peptide mass fingerprinting (PMF) was performed using an Ultraflex III MALDI-TOF/TOF mass spectrometer (Bruker Daltonics, Billerica, MA, USA). Peptide digests without unambiguous PMF identification were further analysed through peptide sequencing by tandem mass spectrometry on an Ultraflex III MALDI-TOF/TOF. Only peptides with individual ion scores of less than 0.05 ($p<0.05$) were considered significant. See Supplementary files for details.

RNA extraction and quantitative RT-PCR (qRT-PCR)

Three independent experiments were carried out using 15 embryos for each exposure. Total RNA was isolated from zebrafish embryos using SV Total RNA Isolation System (Promega, Madison, WI, USA), and each sample was incubated with DNasel to eliminate any genomic DNA residue from the RNA preparation. The 260/280 nM ratio of absorbance was measured with the BioPhotometer spectrophotometer (Eppendorf, Milan, Italy) and used as an indicator of RNA quality and purity. Only the RNAs with a 1.9-2 ratio were considered for further analyses. First-strand cDNAs were synthesized using the ImProm-II Reverse Transcription System (Promega, Madison, WI, USA), following the manufacturer's protocol, using random oligonucleotides to prime the reverse transcription of 1 μg of total RNA. The reactions were performed in a 96-well-format iQ5TM multi-colour real-time PCR detection system (Bio-Rad) using iQTM SYBR® Green Supermix (Bio-Rad). The qPCRs were performed with primers specific for *cyp1a*, *crybb*, *crygn*, *hif1α*, *hif1β*, *hif2α*, *hif2β*, *hif3α*, *hif3β*, *wif1*, *aldh* and *vcp*; for normalization purposes, 18S ribosomal RNA level was tested in all the samples analyzed (see table S1 for primers' sequences). The amplifications were performed as follows: 95 °C for 3 min, then 40 cycles at 95 °C for 10 sec and 58 °C for 30 sec. Three independent qPCR experiments from the same reverse-transcribed sample were performed using each pair of gene-specific primers. The presence of a single PCR product was verified by melting-curve and agarose gel analyses. See Supplementary files for details.

The results of the analyses are expressed as the fold variation (±S.D.) against the controls. A ±2-fold variation was selected as the significance cut-off for the biological effect.

Results

CNPW clean-up and B(α)P adsorption

GC-MS/MS analyses revealed high contamination of the CNPW by PAHs (Fig. S2), accounting for 14 μg/g dry weight (d.w.) and representing 0.0014% of the total carbon mass. After 92 h of toluene extraction, the total PAH content was reduced to only 0.03 μg/g d.w. (0.00003% of the total carbon mass), two orders of magnitude lower than the initially adsorbed PAHs. Thus, we then considered the CNPW cleaned of the toluene-extractable PAHs and ready for contamination by B(α)P.

The GC-MS/MS analyses revealed a negligible B(α)P concentration (0.71 μg/L; 0.071%) in the supernatant and that 33.5% of the administered B(α)P (1 mg/L) was actually adsorbed. The non-adsorbed B(α)P was probably lost mainly during the necessary drying of the suspensions. Anyway, this test proved that the aim of our project design had been reached because we created CNPW to which a significant quantity of B(α)P was adsorbed, without eventual release in water. We calculated a mean B(α)P concentration of 17.2 μg/L adsorbed on 50 mg of CNPW, based on which 20 μg/L B(α)P was then administered during individual exposure assays in order to compare the effects at the same exposure concentrations. The tested concentrations of CNPW and B(α)P did not cause acute effects in zebrafish embryos.

CNPW characterization

SEM revealed many aggregates tens of microns in size in the bulk CNPW (Fig. S3A) with a superficial ultra-structure formed from many graphite-like sheets (Fig. S3B). The bulk CNPW was characterized by aggregates of approximately 10 μm in size that appeared to be constituted by sheets or lamellar-like structures closely attached to one another. TEM characterization of the administered solution revealed two populations of particles: one composed of nanometric graphite-like sheets (Fig. S3C) and another constituted by nanometric particles of approximately 20 nm in size (Fig. S3D).

The dispersion status of the CNPW was evaluated through DLS in terms of the surface charge and hydrodynamic radius (Tab. S2). DLS showed a moderate stability of the CNPW suspension in MilliQ water, which then increased in zfw due to the salts added for zebrafish maintenance.

Microscopy investigations

Light microscopy analyses showed the presence of aggregates associated with the gills both for CNPW administered alone (Fig. 1A) and in co-exposure (Fig. 1C). Figure 1B illustrates the capability of the CNPW particles to pass through the gill cell membranes and accumulate in the epithelium cells (Fig. 1D). We also observed nanometric and electron-dense structures in the nasal fossae (Figs. 2A, C), among the cilia and in their epithelium cells (Figs. 2B, D). Furthermore, large CNPW aggregates were observed in the lumen of the digestive tract (Figs. 3A, C), and the nanometric component was found within microvilli

(Fig. 3B) and internalized in the gastrointestinal wall (Fig. 3D). The nanometric component of CNPW is internalized into red and white blood cells (Figs. 4A, D) for transport to different tissues of the embryo, as proven by the presence of this component in the liver (Figs. 4B, E) and dorsal muscles (Figs. 4C, F). The dimensions of the NPs observed in the organism tissues were approximately 50 nm and ESI verified that NPs were effectively composed of CNPW (Fig. S4). We did not detect any apparent morphological alterations of the target tissues (Fig. 1A, C and Fig. 2A, C) compared with the untreated embryos (Figs. S5, S6).

Indirect immunofluorescence allowed the observation of CNPW (by reflected light) in the gills (Figs. 5I, Q) and in the lumen of the gastrointestinal tract (Figs. 5L, T) both when CNPW was administered alone and in co-exposure. Also B(α)P was located in the same tissues after co-exposure (Figs. 5Q, T). A heavy fluorescence was observed in the yolk when B(α)P was administered alone (Fig. 5N), whilst any signal was detected after co-exposure (Fig. 5R). A similar behaviour was also observed in the digestive tract, in which the signal of B(α)P alone (Fig. 5P) was much higher than that after co-exposure (Fig. 5T). We detected some auto-fluorescent cells into the intestinal wall (Fig. 5T), as well as some natural reflection in the swim bladder probably caused by guanine crystals whose presence was also confirmed by TEM.

Functional proteomics

Figure S7 shows three examples of two-dimensional gels containing the complete protein pattern of the zebrafish embryos. We identified a mean of 2,000 different spots in each analysed gel (n=20): 417 spots were shared between DMSO and B(α)P, 490 between zfw and CNPW, and 499 between zfw and CNPW+B(α)P. Image analyses revealed significant variation of the corresponding control (Student t-test; *p<0,05, **p<0,01) in terms of the volume percentage of 23, 26 and 40 spots, respectively. The final cut-off revealed 6, 8 and 16 varying spots in the three treatments, with a % of the volume that was at least 2-fold different from the controls. Figure S8 highlights the characteristics of the total changed proteins: 20 μg/L B(α)P upregulated 3 different proteins and downregulated the other proteins compared to the DMSO control. CNPW administered at 50 mg/L downregulated 7 different proteins and resulted in the overexpression of only one protein. Finally, co-exposure to CNPW+B(α)P resulted in the significant overexpression of 9 proteins and reduced expression of the other seven proteins. From mass spectrometry data, we were able to identify 5 changed proteins in the zebrafish embryos exposed to 20 μg/L B(α)P, 7 proteins at 50 mg/L CNPW exposure and 14 proteins with co-exposure, whose characteristics were shown in Tables S3, S4, S5.

Gene transcription

The entire dataset is shown in Fig. S9. Modulation of *cyp1a* expression was evaluated first to test the experimental conditions for the embryos' responses. As expected, *cyp1a*

upregulation after B(α)P exposure was observed, whereas no variation and even slight downregulation of *cyp1a* were observed with CNPW and CNPW+B(α)P, respectively.
The *crybb* and *crygn* genes encode β-crystallin and γ-crystallin, respectively. Whereas *crygn* experienced slight upregulation after B(α)P exposure, no variation was observed for *crybb* with B(α)P or CNPW+B(α)P, the latter of which resulted in slight downregulation of *crygn*. Finally, clear downregulation of both *crybb* and *crygn* was noted after CNPW exposure.
Wif1 encodes the wingless-type (Wnt) inhibitory factor 1 protein and was clearly downregulated only by CNPW+B(α)P, whereas the α-aminoadipic semialdehyde dehydrogenase-encoding gene (*aldh*) was downregulated by CNPW and co-exposure.
The *vcp* gene encoding the valosin-containing protein was downregulated only following CNPW exposure.
We analysed the modulation of six *hif* (hypoxia-inducible factors) genes involved in embryonic development and counteracting hypoxia in zebrafish. The *hif1α* and *hif1β* isoforms did not show any fold changes compared to the control for all three treatments, whereas *hif2α* was always downregulated. *hif2β* and *hif3β* were both downregulated after only B(α)P and CNPW exposure. Finally, the *hif3α* isoform was downregulated by only B(α)P.

DISCUSSION

The biological effects of environmental contaminant mixtures have been poorly investigated and are not easy to predict. This is particularly true for the aggregation of physical and chemical pollutants, such as NPs and heavy metals and/or persistent organic pollutants, which possess different intake routes in organisms and various targets and mechanisms of action (Hartmann and Baun, 2010; Canesi et al., 2015). For instance, when CBNs with adsorbed environmental pollutants enter an organism, their fate and effects are varied (Baun et al., 2008; Costa et al., 2012; Su et al. 2013; Ferreira et al., 2014). These differences in intake and toxicological behaviour can be due to the selected model organism, analysed tissues and measured endpoints, as well as interference from the contemporary presence of pollutants administered separately to the organism. In this latter case, three different fractions are available to enter the biological model: the two separate pollutants free in the water phase and their combination. Thus, it is not easy to distinguish the behaviour and effects of each of these fractions from those induced by their association, bearing in mind the possible additive, synergic and antagonistic mechanisms. Thus, our decision to administer only the fraction represented by the previously arranged association to the zebrafish embryos, in addition to administering CNPW and B(α)P separately, helped highlight the B(α)P uptake and transport to diverse embryo compartments only through the compound adsorption to CNPW when in co-exposure.
The interaction between the NPs and cellular membranes is one of the crucial questions in nanotoxicology since their relationship and intake mechanisms are almost unknown. TEM observations allowed us to evaluate how and when NPs can enter organisms, revealing that

CNPW uptake is strictly dependent on its morphological characteristics. The nanometric CNPW (Fig. S3D) was the only component able to pass through the membrane barriers, while the large aggregates found between the gill arches and digestive lumen represented potential sources of NPs that broke off from the coarse substrates (Fig. S3C). TEM investigations revealed another intake pathway for CNPW involving the nasal fossae (Fig. 2) not previously described in zebrafish to the best of our knowledge.

Once the CNPW alone and in co-exposure enters the embryo, the crucial question involves its fate because its transport to other compartments, alone or with adsorbed B(α)P, is not obvious. We found that CNPW was internalized into red and white blood cells (Figs. 4A, D) which then represent potential targets and also specific carriers for the transport of CNPW in other tissues, such as liver (Figs. 4B, E) and dorsal muscles (Figs. 4C, F), demonstrating that CNPW is a multi-target contaminant whose toxic effects are exerted in different organs.

Immunofluorescence furthered understanding of the accumulation of CNPW and the fate of B(α)P, which largely depends on the embryo intake. The results from this analysis highlighted once more the suitability of our experimental design without interference from B(α)P dissolved in water. The fluorescence observed after co-exposure in the gills (Fig. 5Q) and gut (Fig. 5T) was exclusively due to B(α)P transported by the CNPW, whose role as a Trojan-horse carrier was proven by its contemporary presence in the same tissues (Figs. 5Q, T). Moreover, the bioaccumulation of B(α)P was different after individual exposure because high accumulation of the hydrocarbon was observed in the yolk (Fig. 5N), as expected, but no fluorescence was observed in this compartment when administered adsorbed to CNPW (Fig. 5R). These data clearly demonstrate the Trojan-horse mechanism because B(α)P accumulated in yolk lipids after individual exposure but was forced to follow the fate of the CNPW after co-exposure, likely with different biological activity.

To evaluate the biological consequences of the above-mentioned evidence, we assessed the modifications in the zebrafish embryo proteome using high-throughput technology based on functional proteomics supported by gene transcription analysis. Proteomics revealed a completely different effect on biochemical pathways, as indicated by the lack of commonly varied proteins among the three experimental groups (Fig. S8D). Although this is not surprising that B(α)P and CNPW, being chemical and physical pollutants exerting different biological impacts, the absence of commonly altered proteins after co-exposure suggests a modulation of proteins belonging to different cellular targets.

We described the molecular functions of only some proteins and the consequences of their modulation, but complete lists of the varied proteins are shown in Tables S3, S4 and S5. Specifically, B(α)P administered alone generally acted on the expression of certain structural proteins, such as myosins and keratins, with the eye being one of the preferential target organs since two of the three over-expressed proteins, β-crystallin B1 (*Crybb*) and γ-crystallin N-B (*Crygn*), belong to the crystallin family. The expression of βγ–crystallins is believed to be a marker of lens differentiation (Peek et al., 1992) and their expression in the retina suggests a stress-related role. The solubility alteration of crystallins can result in several disorders, such as cataracts, the outcome of partially degraded β-crystallin

polypeptides (David et al., 1993). Indeed, cataracts were also observed in three natural populations of sciaenids from the heavily PAH-polluted Elizabeth River (Virginia, USA) and even induced by the *in vitro* exposure of *Leiostomus xanthurus* to PAH-contaminated sediments from the same aquatic ecosystem (Hargis and Zwerner, 1989), proving that the eye is a target for these hydrocarbons. Our results agree with the data of Huang and co-workers (2014) in which B(α)P exposure induced defects and dysfunctions in visual system development, affecting photoreceptor development-related gene expression in zebrafish embryos. In fact, our gene transcription analysis indicated slight upregulation of *crygn*, which could be responsible for the increase in the amount of protein. By contrast, B(α)P exposure did not modulate *crybb* gene expression and the upregulation of *Crybb* protein was probably due to post-transcriptional modifications. However, both *crybb* and *crygn* were also clearly downregulated after CNPW exposure without any significant variation in crystallin modulations.

As for CNPW and CNPW+B(α)P, proteomics revealed significant changes in proteins mainly involved in the homeostatic response to hypoxia. One example of this type of protein is cofilin-1 (*Cfl1*). This small protein belonging to the actin-depolymerizing factor/cofilin (ADF/cofilins) family significantly decreased after CNPW exposure. Mendelsohn and co-workers (2009) noted the downregulation of muscle *Cfl2* (actually renamed as cofilin-1) in zebrafish embryos subjected to acute anoxia, revealing the adaptation of the cytoskeleton and actin assembly to this type of stress. Additionally, the downregulation of the T-complex protein 1γ (*Tcp1γ*) suggests an embryonic response to hypoxia. Since *Tcp1γ* plays an important role in maintaining oxygen homeostasis (Soung-Hun et al., 2015), the decrease in its activity lowers the cellular requirement for O_2 but can imbalance the correct folding of cytoskeleton proteins at the same time (Dekker et al., 2008). In support of the hypoxia response hypothesis, we also observed modulation of the eukaryotic translation elongation factor 2 (*Eef2*), a ribosomal GTP-dependent translocator (Kaul et al., 2011) that is under the precise and reversible control of oxygen tension. Under hypoxic conditions, the phosphorylation of *Eef2* occurred very rapidly, resulting in a modest translational arrest, which is a pivotal homeostatic response that spares ATP and facilitates cell survival (Romero-Ruiz et al., 2012). On the other hand, cell adaptation to reduce oxygen availability to support homeostatic ATP levels is the main physiological response since even transient O_2 deprivation can produce irreversible cell damage. Furthermore, the non-transcriptional adaptive mechanisms are fundamental to cell survival in the early stages of hypoxia before the *hifs* genes can be transcribed (Weir et al., 2005). Hence, we examined the transcription of six different *hif* isoforms that represent the master regulators of a wide group of genes, whose expression decreases the cellular O_2 demand and inversely increases the O_2 supply (Semenza, 2009). Transcriptional analysis did not reveal any variation after CNPW exposure, whereas slight downregulation of three *hifs* was observed. This apparent contradictory result could be explained by the delay in the transcriptional response when the organism is subjected to short, transient hypoxia, which does not allow sufficient time for a productive transcriptional response (Bennewith and Durand, 2004). The lack of

corresponding changes in *Hif* proteins in response to *hif* gene modulation was well explained in a recent work by Koblitz et al. (2015), who demonstrated that the *hifs* mRNA was not indicative of the simultaneous changes in the expression of the encoded proteins under hypoxia variation. Thus, during our experiments, the zebrafish embryos exposed to CNPW probably underwent slight hypoxia since no evident physiological effects or development delays were observed, suggesting the activation of only the non-transcriptional adaptive mechanism for energy homeostasis.

The potential transient hypoxia of the embryos suggested by the proteome modulation was also confirmed after CNPW+B(α)P exposure, although with different modified proteins. For instance, the transitional endoplasmic reticulum ATPase (valosin-containing protein; *Vcp*) is a key oestrogen receptor (ER) stress protein with a pivotal role in the cellular response to hypoxia (Rao et al., 2004). *Vcp* is involved in a wide variety of ATP-dependent cellular processes, including cell cycle regulation, cell growth and death, membrane fusion and transcriptional regulation (Wang et al. 2004). One of the classical and easiest responses to hypoxia is the decrease in the quantity of ATPases due to the depletion of ATP mainly used for protein synthesis and to maintain the homeostatic intracellular environment through the ion pumping system. This protective mechanism is not free of risk since many other cellular functions can be influenced, such as defects in neuronal outgrowth and neurodegeneration. Imamura and collaborators (2012) identified a protective role of *Vcp* during zebrafish neurodevelopment by degrading polyubiquitinated proteins accumulated in embryo neural tissues. Thus, the significant over-expression of *Vcp* observed after the co-exposure experiment was not related to the necessary decrease in ATPases in response to hypoxia but was probably needed to avoid neuronal developmental abnormalities. On the other hand, Klein and co-workers (2005) found an increasing amount of *Vcp* phosphorylation in the hippocampal region of rats exposed to sustained hypoxia. An increased amount of *Vcp* related to a post-transcriptional modification instead of gene modulation was also highlighted by our results showing a lack of upregulation of *vcp* genes. The fact that our embryos were probably subjected to slight hypoxia was also supported by the over-expression of actins, namely the two α and β isoforms linked to the stationary cytoplasm and remodelling of the cellular structure, respectively. Different angiogenic processes, such as migration, proliferation and differentiation are dependent on isoactin (Durham and Herman, 2009), and a primary hypoxia adaptation is the promotion of angiogenesis (Krock et al., 2011).

Finally, it is interesting to discuss the role played by the two altered proteins in common between the CNPW and CNPW+B(α)P exposures. The wingless-type (*Wnt*) inhibitory factor 1 (*Wif1*) is part of the *Wnt* family that consists of several glycoproteins whose signalling composes the major regulatory cascades of normal embryogenesis, nervous system development and many organ and tissue homeostasis processes (Ciani and Salinas, 2005; Nakaya et al., 2008). The expression alteration of *Wif1* suggests the induction of many development effects probably against the fine-tuning of the spatial and temporal pattern of *Wnt* activity. For instance, it has been demonstrated that the interaction between

Wnts and their antagonists, including *Wif1*, plays a critical role in the early stages of eye development (Stigloher et al., 2006; Tendeng and Houart, 2006). Since the same down-expression of *Wif1* was also observed with co-exposure, in which evident downregulation of the encoding gene was observed, we can suppose a possible effect of CNPW on the transcriptional control of *wif1* expression, which was also partially confirmed by the fold variation (0.6) of the individual exposure at the limit for effective downregulation (threshold=0.5).

The varied protein levels of α-aminoadipic semialdehyde dehydrogenase (*α-Aasa dehydrogenase*) were also similar between the CNPW and CNPW+B(α)P exposures. The *α-Aasa dehydrogenase* is a multifunctional enzyme that mediates important protective effects, such as cell protection against oxidative stress by metabolizing a number of lipid peroxidation-derived aldehydes. Babcock and co-workers (2014) demonstrated that *α-Aasa dehydrogenase* is involved in correct eye development of zebrafish and its downregulation should determine aberrant effects in this organ. This finding highlights again this organ as one of the main targets of the tested contaminants during zebrafish development. This aspect should be considered with special attention in the supposed Trojan-horse mechanism because our dataset demonstrated that the two contaminants and their mixture acted on the same organ but modified different proteins. Here, the expression of *α-Aasa dehydrogenase* was modulated by its encoding gene, *aldh7a1*, which was effectively downregulated by both CNPW alone and CNPW+B(α)P, although the gene downregulation was not followed by a significant difference in the amount of protein.

FINAL REMARKS

Our entire dataset allowed us to suggest a different behaviour and biological responses of B(α)P administered alone and when adsorbed to CNPW. In a realistic scenario, organisms are susceptible to two different fractions of B(α)P. The first fraction consists of the hydrocarbon freely dissolved in water that follows the classical routes of exposure for any lipophilic compound, bioaccumulating in the lipid tissues (Fig. 6, blue lines). This fraction represents, in the early stages of pollutant intake at least, a protective mechanism because it decreases the quantity of contaminant capable of reaching the target tissues. Instead, when B(α)P is adsorbed to CNPW, the hydrocarbon is forced to follow the fate of the physical pollutant in the organism (Fig. 6, red lines). B(α)P is then unable to bioaccumulate in the yolk, being transported directly to other compartments and targeting different biological pathways, as shown by the completely different altered proteins involved in each type of exposure. Thus, our results showed a Trojan-horse "mechanism" because CNPW does not merely acts as carrier for B(α)P, but it appears to modify also the toxicological behaviour of B(α)P through a shift in the bioaccumulation compartments and biological responses rather than an increase in the hydrocarbon concentration in the organism. These findings highlight how nanomaterials represent a great challenge in nano-(eco)toxicology as a result of the many variables that can modify the fate and consequently toxic effects of NPs and adsorbed pollutants.

This study was partially funded by the “Cariplo Foundation”. Grant number 2013-0817.

REFERENCES

Ali U, Syed JH, Mahmood A, Zhang G, Jones KC, Malik RN. 2015. Influential role of black carbon in the soil–air partitioning of polychlorinated biphenyls (PCBs) in the Indus River Basin, Pakistan. Chemosphere 134:172–180.

Babcock HE, Dutta S, Alur RP, Brocker C, Vasiliou V, Vitale S, Abu-Asab M, Brooks BP. 2014. aldh7a1 Regulates eye and limb development in zebrafish. PLoS One 9:e101782.

Baird WM, Hooven LA, Mahadevan B. 2005. Carcinogenic polycyclic aromatic hydrocarbon-DNA adducts and mechanism of action. Environmental and Molecular Mutagenesis 45: 106-114.

Baun A, Srensen SN, Rasmussen RF, Hartmann NB, Koch CB. 2008. Toxicity and bioaccumulation of xenobiotic organic compounds in the presence of aqueous suspensions of aggregates of nano-C_{60}. Aquat Toxicol 86:379–387.

Bennewith KL, Durand RE. 2004. Quantifying transient hypoxia in human tumor xenografts by flow cytometry. Cancer Res 64:6183–6189.

Canesi L, Ciacci C, Balbi T. 2015. Interactive effects of nanoparticles with other contaminants in aquatic organisms: friend or foe? Mar Environ Res 111:128–134.

Ciani L, Salinas PC. 2005. Wnts in the vertebrate nervous system: from patterning to neuronal connectivity. Nat. Rev. Neurosci 6:351–362.

Cornelissen G, Elmquist M, Groth I, Gustafsson O. 2004. Effect of sorbate planarity on environmental black carbon sorption. Environ Sci Technol 38:3574–3580.

Costa CLA, Chaves IS, Ventura-Lima J, Ferreira JLR, Ferraz L, de Carvalho LM, Monserrat JM. 2012. *In vitro* evaluation of co-exposure of arsenium and an organic nanomaterial (fullerene, C_{60}) in zebrafish hepatocytes. Comp Biochem Physiol C-Toxicol Pharmacol 155:206–212.

David LL, Shearer TR, Shih M. 1993. Sequence analysis of lens crystallins suggests involvement of calpain in cataract formation. J Biol Chem 268:1937–1940.

Dekker C, Stirling PC, McCormack EA, Filmore H, Paul A, Brost RL, Costanzo M, Boone C, Leroux MR, Willison KR. 2008. The interaction network of the chaperonin CCT. Embo J 27:1827–1839.

Durham JT, Herman IM. 2009. Inhibition of angiogenesis *in vitro*: a central role for β-actin dependent cytoskeletal remodeling. Microvasc Res 77:281–288.

Ferreira JLR, Lonné MN, França TA, Maximilla NR, Lugokenski TH, Costa PG, Fillmann G, Soares FAA, de la Torre FR, Monserrat JM. 2014. Co-exposure of the organic nanomaterial fullerene C_{60} with benzo(α)pyrene in *Danio rerio* (zebrafish) hepatocytes: evidence of toxicological interaction. Aquat Toxicol 147:76–83.

Hargis WJ, Zwerner DE. 1989. Some effects of sediment-borne contaminants on development and cytomorphology of teleost eye-lens epithelial cells and their derivatives. Mar Environ Res 28:399–405.

Hartmann NB, Baun A. 2010. The nano cocktail: ecotoxicological effects of engineered nanoparticles in chemical mixture. Integr Environ Assess Manag 6:311–313.

Hill AJ, Teraoka H, Heideman W, Peterson RE. 2005. Zebrafish as a model vertebrate for investigating chemical toxicity. Toxicological Sciences 86:6-19.

Huang L, Zuo Z, Zhang Y, Wu M, Lin JJ, Wang C. 2014. Use of toxicogenomics to predict the potential toxic effect of benzo(a)pyrene on zebrafish embryos: ocular developmental toxicity. Chemosphere 108:55–61.

IARC (International Agency for Research on Cancer). 2010. IARC Monographs on the Evaluation of Carcinogenic Risks to Humans. Volume 92: Some Non-heterocyclic Polycyclic Aromatic Hydrocarbons and Some Related Exposures. Edited by IARC, Lyon (France). pp. 853.

Imamura S, Yabu T, Yamashita M. 2012. Protective role of cell division cycle 48 (CDC48) protein against neurodegeneration via ubiquitin-proteasome system dysfunction during zebrafish development. J Biol Chem 287:23047–23056.

Kaul G, Pattan G, Rafeequi T. 2011. Eukaryotic elongation factor-2 (eEF2): its regulation and peptide chain elongation. Cell Biochem Funct 29:227–234.

Kimmel CB, Ballard WW, Kimmel SR, Ullmann B, Schilling TF. 1995. Stages of embryonic development of the zebrafish. Dev Dyn 203:253–310.

Klein JB, Barati MT, Wu R, Gozal D, Sachleben Jr LR, Kausar H, Trent JO, Gozal E, Rane MJ. 2005. Akt-mediated valosin-containing protein 97 phosphorylation regulates its association with ubiquitinated proteins. J Biol Chem 280:31870–31881.

Koblitz L, Fiechtner B, Baus K, Lussnig R, Pelster B. 2015. Developmental expression and hypoxic induction of hypoxia inducible transcription factors in the zebrafish. PloS One 10:e0128938.

Koelmans AA, Jonker MTO, Cornelissen G, Bucheli TD, Van Noort PCM, Gustafsson Ö, 2006. Black carbon: the reverse of its dark side. Chemosphere 63:365–377.

Krock BL, Skuli N, Simon MC. 2011. Hypoxia-induced angiogenesis: good and evil. Genes & Cancer 2:1117–1133.

Limbach LK, Wick P, Manser P, Grass RN, Bruinink A, Stark WJ. 2007. Exposure of engineered nanoparticles to human lung epithelial cells: influence of chemical composition and catalytic activity on oxidative stress. Environ Sci Technol 41:4158–4163.

Mendelsohn BA, Malone JP, Townsend RR, Gitlin JD. 2009. Proteomic analysis of anoxia tolerance in the developing zebrafish embryo. Comp Biochem Physiol D-Genomics Proteomics 4:21–31.

Nakaya N, Lee HS, Takada Y, Tzchori I, Tomarev SI. 2008. Zebrafish olfactomedin 1 regulates retinal axon elongation *in vivo* and is a modulator of Wnt signaling pathway. J Neurosci 28:7900–7910.

Ni M, Huang J, Lu S, Li X, Yan J, Cen K. 2014. A review on black carbon emissions, worldwide and in China. Chemosphere 107:83–93.

Nowack B, Bucheli TD. 2007. Occurrence, behaviour and effects of nanoparticles in the environment. Environ Pollut 150:5–22.

Peek R, McAvoy JW, Lubsen NH, Schoenmakers JG. 1992. Rise and fall of crystallin gene messenger levels during fibroblast growth factor induced terminal differentiation of lens cells. Dev Biol 152:152–160.

Pérez S, Farré M, Barceló D. 2009. Analysis: behaviour and ecotoxicity of carbon-based nanomaterials in the aquatic environment. Trends Anal Chem 28: 820–832.

Rao RV, Poksay KS, Castro-Obregon S, Schilling B, Row RH, Del Rio G, Gibson BW, Ellerby HM, Bredesen DE. 2004. Molecular components of a cell death pathway activated by endoplasmic reticulum stress. J Biol Chem 279:177–187.

Riva C, Binelli A, Rusconi F, Colombo G, Pedriali A, Zippel R, Provini A. 2011. A proteomic study using zebra mussels (*D. polymorpha*) exposed to benzo(α)pyrene: the role of gender and exposure concentrations. Aquat Toxicol 104:14–22.

Romero-Ruiz A, Bautista L, Navarro V, Heras-Garvin A, March-Diaz R, Castellano A, Gomez-Diaz R, Castro MJ, Berra E, Lopez-Barneo J, Pascual A. 2012. Prolyl hydroxylase-dependent modulation of eukaryotic elongation factor 2 activity and protein translation under acute hypoxia. J Biol Chem 287:9651–9658.

Semenza GL. 2009. Regulation of oxygen homeostasis by hypoxia-inducible factor 1. Physiology 24:97–106.

Shrestha G, Traina JS, Swanston WC. 2010. Black carbon's properties and role in the environment: a comprehensive review. Sustainability 2:294–320.

Soung-Hun R, Kasembeli M, Bakthavatsalam D, Chiu W, Tweardy DJ. 2015. Contribution of the type II chaperonin, TRiC/CCT to oncogenesis. Int J Mol Sci 16:26706–26720.

Stigloher C, Ninkovic J, Laplante M, Geling A, Tannhäuser B, Topp S, Kikuta H, Becker TS, Houart C, Bally-Cuif L. 2006. Segregation of telencephalic and eye-field identities inside the zebrafish forebrain territory is controlled by Rx3. Development 133:2925–2935.

Su Y, Yan X, Pu Y, Xiao F, Wang D, Yang M. 2013. Risks of single-walled carbon nanotubes acting as contaminants-carriers: potential release of phenanthrene in Japanese medaka (*Oryzias latipes*). Environ Sci Technol 47:4704–4710.

Tendeng C, Houart C. 2006. Cloning and embryonic expression of five distinct sfrp genes in the zebrafish *Danio rerio*. Gene Expr Patterns 6:761–771.

Wang Q, Song C, Li CC. 2004. Molecular perspectives on p97-VCP: progress in understanding its structure and diverse biological functions. J Struct Biol 146:44–57.

Wang Z, Liu S, Ma J, Qu G, Wang X, Yu S, He J, Liu J, Xia T, Jiang G-B. 2013. Silver nanoparticles induced RNA polymerase-silver binding and RNA transcription inhibition in erythroid progenitor cells. ACSNano 7:4171–4186.

Watson AY, Valberg PA. 2001. Carbon black and soot: two different substances. Am Ind Hyg Ass J 62:218–228.

Weir EK, López-Barneo J, Buckler KJ, Archer SL. 2005. Acute oxygen-sensing mechanisms. N Engl J Med 353:2042–2055.

FIGURE CAPTIONS

Figure 1 CNPW revealed in gills by optical microscopy and TEM.
Semi-thin sections of embryos' zebrafish (96 hpf) gills after CNPW (A) and CNPW+B(α)P exposure (C) visualized by optical microscopy.
Ultra-thin sections of gills' epithelium cell of embryos' zebrafish (96 hpf) after CNPW (B) and CNPW+B(α)P exposure (D) visualized by TEM.
CNPW is indicated by arrows.

Figure 2 CNPW observed in nasal fossae by TEM.
Ultra-thin sections of nasal fossae of zebrafish embryos (96 hpf) after CNPW (A) and CNPW+B(α)P exposure (C).
Ultra-thin sections of the epithelium of nasal fossae of zebrafish embryos (96 hpf) after CNPW (B) and CNPW+B(α)P exposure (D).
CNPW is indicated by arrows.

Figure 3 CNPW observed in gastrointestinal tract by optical microscopy and TEM.
Semi-thin sections of gastrointestinal tract of zebrafish embryos (96 hpf) after CNPW (A) and CNPW+B(α)P exposure (C) visualized by optical microscopy (40X; scale bar: 50 μm). CNPW aggregates are indicated in the red squares.
Observation of CNPW among microvilli after CNPW (B) and CNPW+B(α)P exposure (D) visualized by TEM (scale bar: 2 μm).
CNPW is indicated by arrows.

Figure 4 CNPW observed in blood cells, liver and muscle by TEM.
Aggregates of nanoparticles in a blood red cell after CNPW exposure (A) and in a white blood cell after CNPW+B(α)P exposure (D).
Nanoparticles in liver (B) and muscle (C) after CNPW and CNPW+B(α)P exposures (E, F).
CNPW is indicated by arrows.

Figure 5 Immunofluorescence on different zebrafish embryos. Tissues and experiments are shown in the figure.
In red are shown the F-actine of muscles by phalloidine, the blue signals (DAPI) indicate the nuclei of cells, while B(α)P is coloured in green. Reflection due to CNPW is indicated by squares, yellow arrows show B(α)P accumulation and the asterisks highlight auto-fluorescent cells. Q' is the enlarged portion of the smaller square to indicate better the CNPW aggregates in gills.

Figure 6 Schematic diagram depicting the different pathways followed by B(α)P when administered alone (blue lines) and adsorbed to CNPW (red lines). The main changed protein classes found after the exposures were also shown.

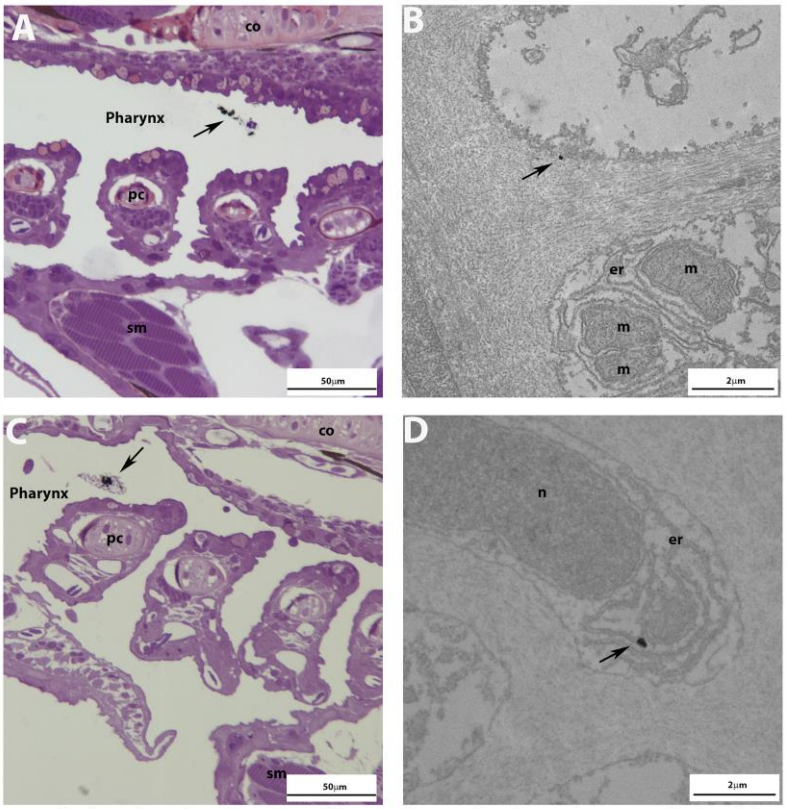

pc= pharingeal cartilage; sm=somatic muscle; co=chondrocranium; m=mitochondrion; er=endoplasmic reticulum; n=nucleus

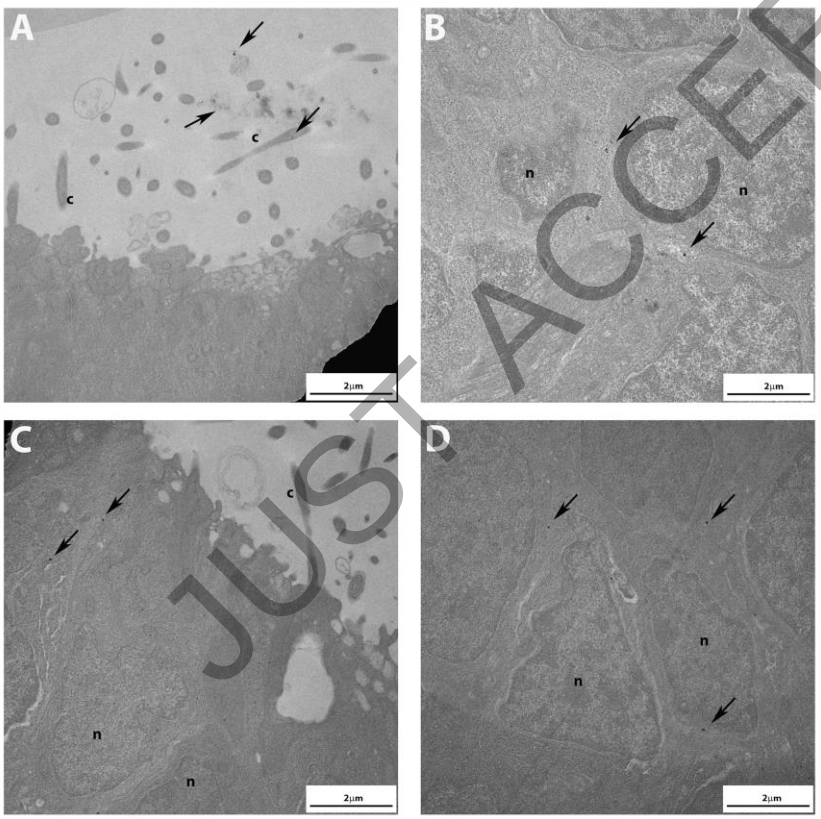

n=nucleus; c=cilium

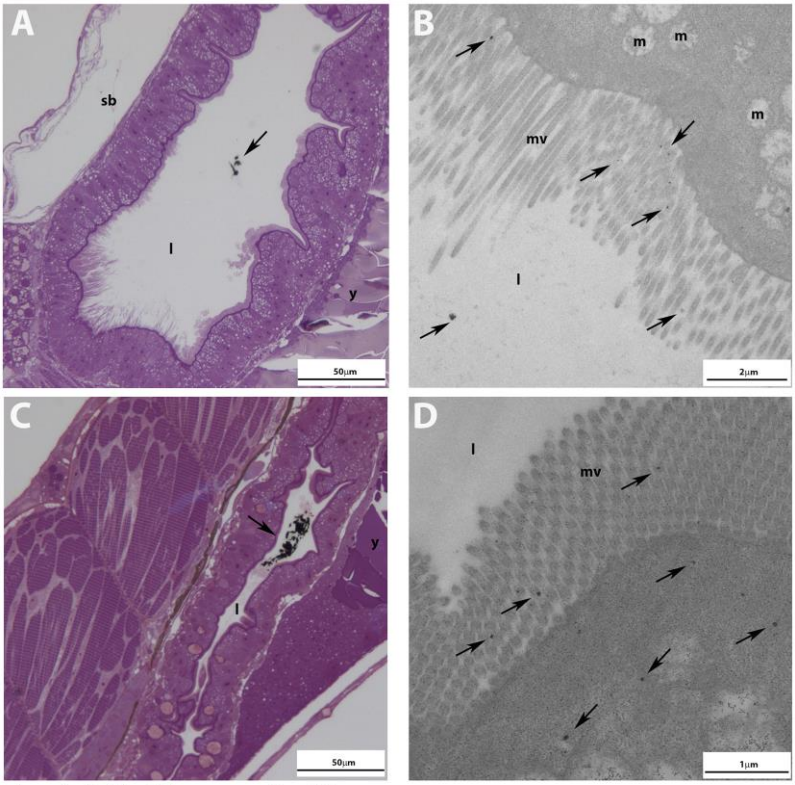

sb=swim bladder; l=lumen; mv=microvilli

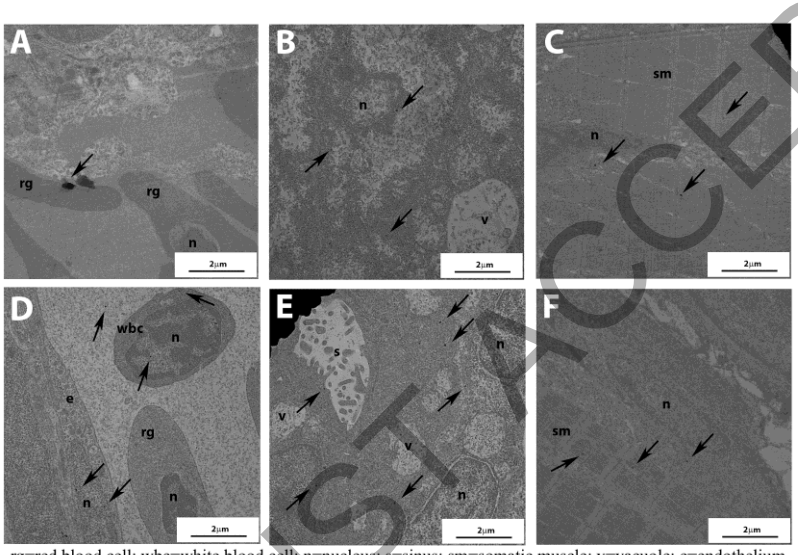

rg=red blood cell; wbc=white blood cell; n=nucleus; s=sinus; sm=somatic muscle; v=vacuole; e=endothelium

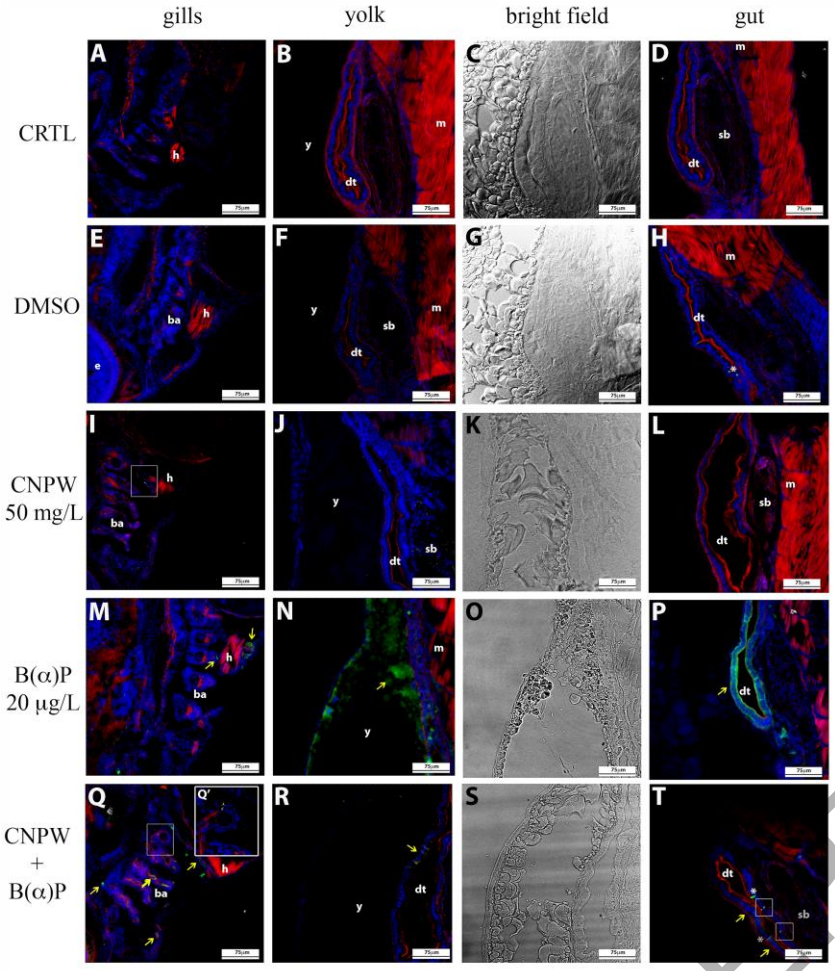

h=heart; ba=branchial arches; e=eye; y=yolk; dt=digestive tract; m=muscle; b=swim bladder